Research Square

Preprints are preliminary reports that have not undergone peer review.
They should not be considered conclusive, used to inform clinical practice,
or referenced by the media as validated information.

Muscle fibre-resolved spatial transcriptomics of regeneration, necrosis and border zones in human paraspinal muscle

MARIJA MEZNARIC

marija.meznaric@mf.uni-lj.si

University of Ljubljana

Žiga Šink

University of Ljubljana

Kaja Blagotinšek Cokan

BIA Separations CRO, Labena Ltd

Uršula Prosenc Zmzljak

BIA Separations CRO, Labena Ltd

Simon Horvat

University of Ljubljana

Nejc Umek

University of Ljubljana

Research Article

Keywords: Spatial transcriptomics, muscle fibre necrosis, muscle regeneration, border zone, toxic myopathy

Posted Date: September 22nd, 2026

DOI: https://doi.org/10.21203/rs.3.rs-10872251/v1

License: This work is licensed under a Creative Commons Attribution 4.0 International License.
Read Full License

Additional Declarations: No competing interests reported.

Abstract

Focal necrotizing lesion fields in human skeletal muscle contain a mosaic of necrotic fibres, regenerative fibres, and morphologically preserved neighbouring fibres, but their fibre-resolved molecular organisation remains poorly defined. We applied targeted Xenium spatial transcriptomics to a human lumbar paraspinal muscle biopsy with toxic myopathy and integrated the analysis with serial post-run hematoxylin and eosin stain, adult and neonatal myosin heavy-chain isoforms, immunostaining for membrane attack complex of complement (C5b9) and manual fibre-level region-of-interest segmentation. Distant normal type 1 and type 2 fibres, necrotic fibres, regenerative fibres, and intact type 1 and type 2 fibres immediately adjacent to necrosis or regeneration were compared. Baseline transcriptional differences between distant normal type 1 and type 2 fibres were modest, whereas lesion-associated contrasts were substantially broader, indicating that pathological state outweighed basal fibre identity within this targeted panel. Necrotic fibre regions were enriched for immune/myeloid-associated transcripts, including *PLA2G7*, *TREM2*, *FCGR3A*, *MS4A4A*, *CD163*, *MRC1*, and *PTPRC*, whereas regenerative fibres preferentially expressed structural and calcium-handling genes, including *MYBPC1*, *DES*, *MEF2C*, *S100A1*, and *PVALB*. Despite preserved morphology, fibres bordering necrosis displayed a pronounced border-zone signature that largely overlapped the necrotic programme, whereas neighbourhood effects around regeneration were weaker and fibre-type dependent. These findings define necrosis, regeneration, and their border zones as distinct spatial states within a focal human muscle lesion and indicate that fibres adjacent to necrosis, despite being morphologically normal, are unsuitable internal comparators.

Introduction

Acute necrotizing muscle injury is spatially heterogeneous at the level of individual muscle fibres, with necrotic fibres, regenerative fibres, and morphologically preserved neighbouring fibres often coexisting within the same field. This pattern is encountered across toxic and immune-mediated necrotizing myopathies, which share a common morphological triad of muscle fibre necrosis, macrophage-predominant clearance, and regeneration with reactivation of developmental programmes (Pinal-Fernandez and Mammen 2016; Tidball 2017). Cocaine-associated myopathy represents one clinically relevant setting in which such focal lesion fields may arise, likely through multifactorial injury including direct myotoxicity, vasoconstriction-related ischaemia, hyperthermia, and excessive muscular activity (Nolte 1991; Selvaraj et al. 2013; Pasnoor et al. 2014; Doughty and Amato 2019). Conventional histopathology and immunohistochemistry define these lesions morphologically, but they provide only a partial view of molecular states within individual fibres and their immediate border zones.

Skeletal muscle fibres differ markedly in sarcomeric organisation, metabolism, excitation-contraction coupling, and contractile performance (Schiaffino and Reggiani 2011). Slow/type 1 and fast/type 2 fibres express different myosin heavy-chain isoforms, whereas hybrid fibres co-express isoforms and may become more prominent during remodelling or fibre-type transitions (Pette and Staron 2000), although they are also present in normal human muscle (Williamson et al. 2001; Meznaric and Cvetko 2016;

Meznaric et al. 2018). Single-fibre transcriptomic studies in human muscle further show that slow and fast fibres have distinct basal gene-expression signatures (Chemello et al. 2011; Murgia et al. 2021; Umek et al. 2025). These intrinsic differences raise the possibility that both fibre identity and local lesion context shape transcriptional responses to acute muscle injury.

Spatial transcriptomic technologies can link gene expression to tissue architecture, enabling molecular dissection of pathological niches that remain unresolved by bulk or dissociated profiling (Ståhl et al. 2016). In skeletal muscle, spatial transcriptomics has begun to reveal spatially organised functional domains and injury responses (D'Ercole et al. 2022). Recent human studies of inflammatory myopathies have likewise identified spatially restricted damage niches enriched for immune signatures and altered muscle fibre-associated states, underscoring the relevance of spatial context in muscle pathology (Wischnewski et al. 2024). However, fibre-resolved molecular comparisons of necrotic fibres, regenerative fibres, and morphologically intact neighbouring fibres within the same focal human lesion field remain limited.

In this study, we applied targeted Xenium in situ spatial transcriptomics to a focal lesion field in human paraspinal muscle affected by cocaine-associated myopathy, using an assay and workflow aligned with our previously described human skeletal muscle Xenium protocol (Umek et al. 2025). We integrated morphology with fibre-level region-of-interest (ROI) transcript profiles representing necrotic fibres, regenerative fibres, morphologically normal type 1 and type 2 fibres distant from pathology, and type 1 and type 2 fibres immediately adjacent to necrosis or regeneration. This design enabled direct comparison of injury, repair, and border-zone states within the same focal lesion while preserving fibre-type context. We aimed to define molecular programmes distinguishing necrosis from regeneration, to determine basal fibre-type signatures in morphologically normal tissue distant from lesions, and to examine whether fibres neighbouring necrosis or regeneration retain a normal transcriptional state or already exhibit local lesion-associated remodelling.

Materials and methods

Tissue sample and cryosectioning

We investigated molecular organisation of focal necrotizing lesions in toxic myopathy. A diagnostic open surgical biopsy specimen of the superficial left lumbar paraspinal muscle from a middle-aged person with a documented history of cocaine use and acute myopathy was taken on June 2023, snap-frozen in liquid nitrogen and, after a diagnostic work-up, stored in liquid nitrogen in the Neuromuscular Tissue Bank of the University of Ljubljana, located at the Institute of Anatomy, Faculty of Medicine; the bank is a partner of the EuroBioBank (Mora et al. 2015) and BBMRI-ERIC (Holub et al. 2016) networks. Written informed consent was obtained before the diagnostic surgical biopsy procedure. Only author MM has access to information that could identify the individual participant during and after data collection. On May 2024 transverse cryosections (10 µm) of the archived sample were cut on a Leica CM1950 cryostat

(Leica Microsystems, Germany), with the blade set to -20°C and the specimen head to -10°C. Sections were stored at -80°C until downstream assays.

Xenium in situ gene expression assay

Spatial transcriptomic profiling was performed with the 10x Genomics Xenium In Situ Gene Expression workflow for fresh-frozen tissue. The Human Multi-Tissue and Cancer Panel targeting 377 genes was used. Overall, sample preparation and acquisition followed our previously described Xenium workflow for human skeletal muscle (Umek et al. 2025). A morphology check was performed before section placement. Tissue sections were mounted on Xenium slides with a 12 mm × 24 mm imageable area and a 10.45 mm × 22.45 mm sample-positioning area. Fresh-frozen tissues were fixed and permeabilised using Sample Pre-Reagents (10x Genomics, PN 1000626). Probe hybridisation with the Human Multi-Tissue and Cancer Panel (10x Genomics, PN 1000626) was performed overnight, followed by ligation and rolling circle amplification to generate gene-specific barcodes for in situ imaging.

For multimodal staining, the Multimodal Tissue Segmentation Kit (10x Genomics, PN 1000661) was used. The kit provided DAPI for nuclei, S18 RNA for cytoplasmic signal, and antibodies against ATP1A1, CD45, and E-cadherin for membrane staining. Data were acquired on a Xenium Analyzer using instrument software v2.0.1.0 and analysis software Xenium-2.0.0.10, yielding cell-by-gene and transcript-by-location matrices.

Post-run histology

Following Xenium acquisition, the same section was stained with hematoxylin and eosin (H&E) (Fig. 1a, b) using the recommended post-run workflow to verify tissue integrity and support pathological annotation of necrotic and regenerative fibres and their surrounding endomysial, perimysial, and vascular compartments.

MyHC immunohistochemistry and morphometry

Serial transverse cryosections were immunostained with BA-D5 and SC-71 monoclonal antibodies (Fig. 1c, d) specific for myosin heavy chains MyHC1 and MyHC2a/2x, respectively (DSMZ, Germany). Fibres were classified as type 1, type 2, or hybrid; hybrid fibres showed concurrent BA-D5 and SC-71 immunoreactivity, whereas fibres with absent or ambiguous staining were classified as “other” for composition analyses. Additional serial sections were stained for neonatal myosin heavy chain (Fig. 1e) (MyHC neo, Leica Biosystems, UK) to identify regenerative fibres. Necrotic fibres were evaluated on serial sections stained for C5b9 deposition (Fig. 1f) (Dako, Denmark). Antigen detection was performed by an indirect immunoperoxidase method with the P0260 secondary antibody, as described previously (Cvetko et al. 2012; Meznaric and Cvetko 2016). Morphometry was performed on morphologically normal muscle fibres. Two fields of view were selected on serial sections: one adjacent to necrotic and

regenerative fibres and one distant from such lesions. Individual fibres were manually delineated in Ellipse, and the minimal Feret diameter and cross-sectional area were extracted for each fibre. Fibre-type assignment was supported by previously described software (Karen et al. 2009).

Region-of-interest definition and manual muscle fibre segmentation

Xenium outputs were inspected in Xenium Explorer (v3.0). Because skeletal muscle fibres are multinucleated and closely juxtaposed to mononuclear cells, automated cell segmentation was not used for fibre-level quantification. Instead, muscle fibre ROIs were delineated manually using membrane-associated signal as a boundary guide and cross-checked against the post-run H&E image and serial MyHC and C5b9 immunostaining. ROIs were assigned to eight biologically defined groups: morphologically normal type 1 fibres distant from pathology, morphologically normal type 2 fibres distant from pathology, necrotic fibres, regenerative fibres, type 1 fibres adjacent to necrosis, type 2 fibres adjacent to necrosis, type 1 fibres adjacent to regeneration, and type 2 fibres adjacent to regeneration. Necrotic fibres were identified on H&E and C5b9-stained sections, whereas regenerative fibres were identified on serial sections stained for neonatal MyHC. Hybrid and “other” fibres were excluded from Xenium ROI comparisons. In total, 204 fibre ROIs were analysed: 49 distant normal type 1 fibres, 49 distant normal type 2 fibres, 26 necrotic fibres, 16 regenerative fibres, and 16 fibres in each neighbouring group. In an exploratory analysis, necrotic fibres were further stratified by C5b9 immunoreactivity (C5b9 + vs C5b9−).

Transcript density quantification and normalisation

Transcript density was defined as the number of detected transcripts per ROI area (transcripts/μm²). For gene-level comparisons, per-gene transcript densities were additionally expressed relative to the total transcript density of the same ROI, yielding normalised transcript densities for downstream two-group analyses. For each two-group comparison, log2 fold-changes were calculated from group mean normalised transcript densities (log2[meanA/meanB]). Genes with a zero mean in one group were reported as detected only in the other group in the supplementary tables.

Statistical analysis

Statistical analyses were performed in GraphPad Prism (v10) unless otherwise stated. For morphometric comparisons between morphologically normal fibres in regions adjacent to pathology and those in distant normal regions, continuous variables were compared using the Mann-Whitney U test. Fibre-type proportions were compared using Fisher’s exact test, and the overall fibre-type distribution was compared using a chi-square test. Total transcript density across ROI groups was analysed using prespecified pairwise Mann-Whitney U tests, with two-stage step-up false discovery rate correction of Benjamini, Krieger, and Yekutieli (Benjamini et al. 2006) across all planned comparisons. Gene-level differential analyses between two ROI groups were performed using Mann-Whitney U tests on normalised transcript densities, with the same FDR procedure applied across the 377-gene panel. Unless

stated otherwise, $q < 0.01$ was considered significant. Neighbourhood overlap analyses were based on intersections of FDR-significant gene sets across relevant contrasts.

Results

Morphologically normal tissue adjacent to lesions shows altered fibre-type composition without size remodelling

We analysed 49 morphologically normal fibres from regions adjacent to necrosis and regeneration and 95 morphologically normal fibres from distant regions (Table 1). Adjacent regions contained fewer type 1 fibres (16.3% vs 34.7%, $p = 0.021$), while the proportion of type 2 fibres did not differ significantly (59.2% vs 63.2%, $p = 0.718$). Hybrid or other fibres were more frequent in adjacent regions (24.5% vs 2.1%, $p = 4.44 \times 10^{-5}$), and the overall fibre-type distribution also differed between regions ($p = 3.38 \times 10^{-5}$). Minimal Feret diameter and cross-sectional area did not differ significantly. Median minimal Feret diameter was 56.17 µm in adjacent regions and 49.56 µm in distant regions (p = 0.468), while median cross-sectional area was 3123.9 µm² and 3704.4 µm², respectively ($p = 0.159$).

Table 1
Fibre-type composition and morphometry of morphologically normal fibres in regions adjacent to versus distant from necrosis and regeneration

Metric	Adjacent normal fibres (n = 49)	Distant normal fibres (n = 95)	Overall *p* value
Type 1 fibres, n (%)	8 (16.3%)	33 (34.7%)	0.021
Type 2 fibres, n (%)	29 (59.2%)	60 (63.2%)	0.718
Hybrid or other fibres, n (%)	12 (24.5%)	2 (2.1%)	4.44 × 10⁻5
Minimal Feret diameter, median (IQR), µm	56.17 (30.21–66.08)	49.56 (42.48–58.06)	0.468
Cross-sectional area, median (IQR), µm²	3123.9 (993.6–4622.3)	3704.4 (3006.9–4404.8)	0.159

Hybrid fibres showed concurrent BA-D5 and SC-71 reactivity, whereas “other” fibres had ambiguous or no detectable staining. The overall *p* value of the chi-square comparison across the three fibre categories was 3.38×10^{-5}.

Pathological state exceeds baseline fibre-type differences

Pathological ROIs occupied a higher-transcript-density state than morphologically intact fibres. Necrotic fibres showed the highest mean transcript density (1.8816 transcripts/µm²), followed by regenerative fibres (1.7364 transcripts/µm²); these two groups did not differ significantly from each other (q = 0.143),

but both exceeded all morphologically intact categories. Within distant normal tissue, type 1 fibres also showed higher transcript density than type 2 fibres (0.7838 vs 0.6141 transcripts/μm²; $q = 5.94 \times 10^{-7}$).

C5b9 status does not define a separate necrotic state

Membrane attack complex of complement (C5b9) deposition did not identify a separate necrotic transcriptomic subtype. No transcripts differed between C5b9-positive and C5b9-negative necrotic fibres at FDR $q < 0.01$ (Supplementary Table S1). Although the strongest nominal signals in C5b9-positive fibres were directionally compatible with a more immune-enriched niche, all morphologically necrotic fibres were pooled for the primary analyses.

Compared with the modest separation between distant normal type 1 and type 2 fibres, lesion-associated contrasts produced substantially broader transcriptomic shifts. Distant normal type 1 versus type 2 fibres differed by 35 FDR-significant transcripts (Supplementary Table S2), whereas pathology-related comparisons yielded up to 264 significant transcripts. The largest shifts were observed when necrotic or regenerative fibres were compared with distant normal fibres, indicating that, within this targeted panel, pathological state and local lesion context outweighed basal fibre-type identity.

Baseline fibre-type signatures are modest and attenuated near lesions

Basal fibre-type differences were readily detectable in distant normal tissue (Fig. 2a) but remained relatively circumscribed. Thirty-five transcripts differed between distant normal type 1 and type 2 fibres at FDR $q < 0.01$, with type 1 fibres relatively enriched for *PROX1, KCNMA1, TFPI, ADAMTS1, LPL, MYH11*, and *CNN1*, and type 2 fibres for *PEBP4, PMP22, ESR1, PGR*, and *AR* (Supplementary Table S2).

This fibre-type separation was largely blunted in lesion-adjacent tissue. Around necrosis, only *PROX1* and *KCNMA1* remained differential between neighbouring type 1 and type 2 fibres, and around regeneration, only *PROX1* remained significant (Supplementary Tables S3 and S4). These findings indicate partial convergence of local transcriptional states in fibres exposed to pathological microenvironments.

Necrotic and regenerative fibres define distinct immune and repair states

Necrotic and regenerative fibres occupied clearly distinct molecular states (Fig. 2b). A total of 111 transcripts differed between the two groups at FDR $q < 0.01$ (Supplementary Table S5). Necrotic fibre ROIs were relatively enriched for immune/myeloid-associated transcripts, including *PLA2G7, TREM2, FCGR3A, MS4A4A, CD163, MRC1*, and *PTPRC*, suggesting the presence of a macrophage-rich environment. Given the close spatial association of infiltrating immune cells with damaged muscle fibres, these signals likely reflect the local lesion microenvironment at least in part and should therefore not be interpreted as exclusively muscle fibre-intrinsic transcription. In contrast, regenerative fibres preferentially expressed genes linked to contractile reassembly and calcium handling, including *MYBPC1, DES, MEF2C, S100A1*, and *PVALB*. Relative to distant normal tissue, the broadest lesion-associated shift

was observed for necrotic versus distant normal type 2 fibres (264 transcripts), with a somewhat smaller but still extensive separation for regenerative versus distant normal type 2 fibres (139 transcripts) (Supplementary Tables S6 and S7).

Necrotic transcriptional spillover is strong, whereas regenerative neighbourhood effects are limited

Despite preserved morphology, fibres bordering necrosis already displayed a molecular phenotype that closely paralleled the necrotic lesion itself (Fig. 2c, e). Type 2 fibres adjacent to necrosis differed from distant normal type 2 fibres by 41 transcripts at FDR $q < 0.01$, all of which overlapped the necrotic-versus-distant-normal type 2 signature; type 1 fibres adjacent to necrosis differed from distant normal type 1 fibres by 37 transcripts, 35 of which overlapped the corresponding necrotic contrast (Supplementary Tables S8 and S9). Representative genes included *CD86*, *MNDA*, *CD14*, *CD4*, *CXCR4*, *SPI1*, *VSIG4*, *MRC1*, *FCGR3A*, and *PTPRC*, consistent with a strong local necrotic field effect.

By comparison, neighbourhood effects around regeneration were weaker and fibre-type dependent (Fig. 2d, f). Type 1 fibres adjacent to regeneration differed from distant normal type 1 fibres by 23 transcripts at FDR $q < 0.01$, including *SFRP2*, *ERBB2*, *ASPN*, *VCAN*, and *PTGDS*, whereas type 2 fibres adjacent to regeneration showed no FDR-significant differences at the predefined threshold (Supplementary Tables S10 and S11). Direct comparison of fibres adjacent to necrosis versus regeneration identified only *SPI1* in type 2 neighbours, while no FDR-significant genes separated the two groups in type 1 neighbours (Supplementary Tables S12 and S13).

Complementary lesion-versus-reference contrasts using distant normal type 1 fibres likewise showed broad separation, with 240 FDR-significant transcripts in the distant normal type 1 versus necrotic comparison and 130 in the distant normal type 1 versus regenerative comparison (Supplementary Tables S14 and S15).

Discussion

Fibre-resolved Xenium profiling of this focal human lesion indicates that cocaine-associated necrotizing muscle injury is not adequately described as a simple dichotomy of damaged and preserved tissue. Rather, within the analysed focal lesion, necrotic fibres, regenerative fibres, and morphologically intact neighbouring fibres occupied spatially distinct molecular states, with the strongest intermediate state observed at the necrotic border zone. Within the limits of the targeted 377-gene panel, baseline fibre-type differences in distant normal tissue were relatively modest, whereas lesion-associated contrasts were substantially broader. This pattern indicates that, in the present dataset, local pathological context outweighed basal fibre identity. The most important spatial finding was that fibres immediately adjacent to necrosis already displayed an abnormal transcriptional state despite preserved morphology. By integrating spatial transcriptomics with fibre-level segmentation, the present approach enables these molecular states to be interpreted directly in the anatomical context of individual fibres and their local injury microenvironment.

Regions adjacent to necrotic and regenerative fibres also differed from distant normal tissue at the morphometric level, although the pattern was one of altered composition rather than overt size remodelling. Adjacent regions contained fewer type 1 fibres and more hybrid or other fibres, whereas minimal Feret diameter and cross-sectional area did not differ significantly. The excess of hybrid fibres may reflect local myosin isoform transitions during remodelling, although this interpretation remains tentative (Pette and Staron 2000). The increase in the “other” category may likewise reflect weak, heterogeneous, or ambiguous MyHC immunoreactivity and should therefore be interpreted cautiously. Importantly, the absence of a region-wide shift in fibre size does not argue against active injury and repair, because fibre necrosis and regenerative replacement can occur asynchronously within the same focal lesion (Chargé and Rudnicki 2004; Tidball 2017). Taken together, these morphometric findings are more consistent with local phenotypic heterogeneity than with diffuse remodelling of the surrounding muscle (Schiaffino and Reggiani 2011; Esbjörnsson et al. 2021).

Pathological ROIs also occupied a substantially higher-transcript-density state than morphologically intact ROIs, with necrotic and regenerative fibres at the upper end of the distribution. This likely reflects not only altered fibre biology but also the dense cellular environment that accompanies injury. In skeletal muscle, necrosis and regeneration are embedded in a coordinated tissue response that includes macrophage-rich debris clearance, satellite-cell activation, and remodelling of injured fibres and their immediate surroundings (Chargé and Rudnicki 2004; Schiaffino et al. 2015; Tidball 2017). Accordingly, part of the increased transcript density in pathological ROIs probably reflects local admixture from tightly apposed non-myofibre cells. At the same time, the higher transcript density observed in distant normal type 1 than in distant normal type 2 fibres is in keeping with basal fibre-type differences and with our previous Xenium analysis of human skeletal muscle (Umek et al. 2025). The present data therefore suggest that total ROI transcript density reflects both biological state and local cellular composition and should not be interpreted as a purely myofibre-intrinsic property.

Necrotic and regenerative ROIs formed clearly separable transcriptional states. Necrotic fibre ROIs were enriched for immune/myeloid-associated transcripts such as *PLA2G7*, *TREM2*, *FCGR3A*, *MS4A4A*, *CD163*, *MRC1*, and *PTPRC*, whereas regenerative fibres preferentially expressed structural and calcium-handling genes including *DES*, *MYBPC1*, *MEF2C*, *S100A1*, and *PVALB*. This separation is biologically plausible. Macrophage-rich clearance of necrotic fibres is a defining feature of acute muscle injury, and immune-associated pathways are therefore expected to dominate the necrotic niche even in the absence of overt vasculitis (Nolte 1991; Pinal-Fernandez and Mammen 2016; Tidball 2017). By contrast, regeneration recapitulates developmental and repair programmes characterised by satellite-cell activation, myogenic differentiation, and progressive reassembly of the contractile apparatus (Chargé and Rudnicki 2004; Schiaffino et al. 2015). Within the limits of the targeted panel, the relative enrichment of contractile and excitation-contraction transcripts in regenerative ROIs is therefore consistent with restoration of fibre structure and function during repair (Chargé and Rudnicki 2004; Schiaffino and Reggiani 2011). At the same time, the presence of transcripts such as *TREM2*, *CD163*, *MRC1*, and *FCGR3A* within necrotic fibre ROIs should not be interpreted as direct evidence of fibre-intrinsic expression, because these signals

likely reflect, at least in part, the close spatial apposition of degenerating fibres and infiltrating immune cells.

One of the most consequential observations was the strong necrotic spillover signature in morphologically intact neighbouring fibres. In the present study, “neighbourhood effects” refer to transcriptional alterations detected in fibres that appear structurally preserved but lie immediately adjacent to a lesion within the same local injury field. The near-complete overlap between neighbour signatures and the necrotic signature indicates that fibres bordering necrosis are not molecularly equivalent to distant normal fibres. Several, not mutually exclusive, explanations are possible. Some neighbouring fibres may represent an early stage of injury following an acute toxic-ischaemic insult, before overt structural breakdown becomes morphologically apparent (Nolte 1991; Pasnoor et al. 2014). Others may be responding to soluble mediators, phagocytic activity, or matrix changes generated during necrotic clearance (Chargé and Rudnicki 2004; Tidball 2017). In addition, because ROI-based profiling cannot completely exclude transcripts from tightly apposed mononuclear cells, part of the signal probably reflects local cellular admixture rather than exclusively altered myofibre transcription (Wischnewski et al. 2024; Marco Salas et al. 2025). Regardless of the precise mechanism, the biological implication is clear: fibres adjacent to necrosis should not be treated as molecularly normal internal comparators.

The exploratory comparison of C5b9-positive and C5b9-negative necrotic fibres did not identify any FDR-significant transcripts. The strongest nominal signals in C5b9-positive fibres were directionally compatible with a more immune-enriched niche, but the absence of FDR-significant genes and the small sample size argue against overinterpretation. In practical terms, these data do not support the existence of a clearly separable necrotic transcriptomic subtype defined by C5b9 status within the present panel and sample size. We therefore pooled C5b9-positive and C5b9-negative necrotic fibres in the primary analyses.

In contrast to the robust spillover around necrosis, neighbourhood effects around regeneration were weaker and fibre-type dependent. Type 1 fibres adjacent to regeneration showed 23 significant differences relative to distant normal type 1 fibres, whereas type 2 fibres adjacent to regeneration showed none at the predefined false discovery rate threshold. Direct comparison of fibres adjacent to necrosis and regeneration identified only *SPI1* in type 2 neighbours, and no genes reached the false discovery rate threshold in type 1 neighbours. One plausible explanation is that regenerative foci represent a later, less inflammatory, or less immune-dense local state than actively necrotic foci and therefore exert weaker transcriptional influence on neighbouring intact fibres. Another possibility is that baseline differences between slow and fast fibres influence how strongly local cues are registered or retained, as suggested by single-fibre and spatial studies of human muscle disease (Chemello et al. 2011; Wischnewski et al. 2024). Although these interpretations remain provisional, the asymmetry between necrotic and regenerative neighbourhoods suggests that local lesion effects are not uniform and may depend on both lesion state and fibre identity.

From a broader pathological perspective, these findings are relevant because toxic myopathies, including cocaine myopathy, are usually managed by supportive care and withdrawal of the suspected offending agent, yet the molecular events that distinguish reversible from irreversible local injury remain poorly defined (Selvaraj et al. 2013; Pasnoor et al. 2014). The present data suggest that pathological processes are not confined to overtly necrotic fibres but extend into morphologically intact neighbours, producing an altered local transcriptomic state that may precede, accompany, or follow visible structural injury. This observation has practical implications for tissue interpretation: in focal necrotizing lesions, apparently intact nearby fibres cannot automatically be assumed to represent an internal baseline. More broadly, the results support the idea that lesion organisation in acute toxic muscle injury includes a biologically relevant border zone rather than only sharply separated damaged and undamaged compartments.

Interpretation of these data should, however, consider the design constraints of the study. The Xenium panel used here captures key markers of fibre identity, regeneration, and immune activity, but it does not comprehensively resolve the wider metabolic, stress-response, or extracellular matrix programmes of skeletal muscle. Consequently, the present analysis should be understood as a targeted rather than exhaustive view of lesion biology. In addition, ROI-based profiling cannot perfectly separate myofibre-intrinsic transcripts from those of tightly apposed non-myofibre cells, so part of the border-zone signal may reflect local transcript admixture (Marco Salas et al. 2025). The analysis is also limited to one anatomically defined biopsy from one patient, which constrains generalisability and prevents formal assessment of inter-lesion or inter-patient variability. Finally, the cross-sectional design precludes temporal ordering of necrosis, regeneration, and neighbouring-fibre responses.

Notwithstanding these limitations, the present dataset provides a spatially resolved molecular map of a focal toxic muscle lesion and establishes a framework for testing fibre-level hypotheses in human necrotizing myopathy. Future studies in additional lesion fields and patients should help identify the cellular sources of immune-associated transcripts and distinguish genuinely myofibre-intrinsic border-zone changes from signals driven by local cellular admixture. When combined with orthogonal immunostaining or spatial protein assays, such analyses may also clarify whether necrotic spillover signatures are associated with lesion progression or resolution (Wischnewski et al. 2024). Such work will be needed to determine how broadly the present spatial patterns apply across focal toxic and necrotizing muscle injuries.

Conclusions

In summary, Xenium profiling of a focal lesion in human paraspinal muscle shows that cocaine-associated myopathy comprises distinct necrotic, regenerative and neighbouring states. Necrosis was associated with an immune/myeloid-rich transcriptional milieu, regeneration with structural and excitation-contraction programmes, and fibres adjacent to necrosis already displayed a necrosis-like signature despite preserved morphology. These findings indicate that neighbouring fibres near necrosis

are unsuitable internal comparators in focal toxic myopathy and support fibre-resolved spatial profiling for studying lesion organisation, progression and repair.

Declarations

Acknowledgments and Funding Information

We thank Majda Črnak Maasarani for technical support and Chiedozie K. Ugwoke for critical proofreading of the manuscript. This work was supported by the Slovenian Research and Innovation Agency (ARIS; P3-0043 and P4-0220).

Competing interests

The authors declare no competing interests.

Ethics approval

The study protocol was approved by the National Medical Ethics Committee of the Republic of Slovenia (approval no. 106/07/2010). All procedures were performed in accordance with the ethical standards laid down in the 1964 Declaration of Helsinki and its later amendments.

Consent to participate

Written informed consent was obtained from the patient before the diagnostic surgical biopsy procedure.

Author Contribution

NU developed the concept and study design, supervised the work, interpreted data, and drafted and revised the manuscript; SH co-developed the concept, supervised the study, interpreted data, and revised the manuscript; MM performed microscopy, fibre typing, and manual fibre and ROI delineation, and revised the manuscript; ŽŠ prepared muscle sections, performed immunohistochemistry, microscopy and fibre typing, prepared figures, and revised the manuscript; KBC and UPZ performed Xenium analyses, contributed to methodology, and revised the manuscript. All authors approved the final manuscript.

Acknowledgement

We thank Majda Črnak Maasarani for technical support and Chiedozie K. Ugwoke for critical proofreading of the manuscript.

Data Availability

Gene-level differential-expression summary tables are provided as Supplementary Tables S1–S15. Additional data supporting the findings of this study are available from the corresponding author upon reasonable request.

References

1. Benjamini Y, Krieger AM, Yekutieli D (2006) Adaptive linear step-up procedures that control the false discovery rate. Biometrika 93:491–507. https://doi.org/10.1093/biomet/93.3.491
2. Chargé SBP, Rudnicki MA (2004) Cellular and molecular regulation of muscle regeneration. Physiol Rev 84:209–238. https://doi.org/10.1152/physrev.00019.2003
3. Chemello F, Bean C, Cancellara P, Laveder P, Reggiani C, Lanfranchi G (2011) Microgenomic analysis in skeletal muscle: expression signatures of individual fast and slow myofibers. PLoS ONE 6:e16807. https://doi.org/10.1371/journal.pone.0016807
4. Cvetko E, Karen P, Eržen I (2012) Myosin heavy chain composition of the human sternocleidomastoid muscle. Ann Anat 194:467–472. https://doi.org/10.1016/j.aanat.2012.05.001
5. D'Ercole C, D'Angelo P, Ruggieri V, Proietti D, Virtanen L, Parisi C, Riera CS, Renzini A, Macone A, Marzullo M, Ciapponi L, Bonvissuto D, Sette C, Giordani L, Madaro L (2022) Spatially resolved transcriptomics reveals innervation-responsive functional clusters in skeletal muscle. Cell Rep 41:111861. https://doi.org/10.1016/j.celrep.2022.111861
6. Doughty CT, Amato AA (2019) Toxic myopathies. Continuum (Minneap Minn) 25:1712–1731. https://doi.org/10.1212/CON.0000000000000806
7. Esbjörnsson ME, Dahlström MS, Gierup JW, Jansson EC (2021) Muscle fiber size in healthy children and adults in relation to sex and fiber types. Muscle Nerve 63:586–592. https://doi.org/10.1002/mus.27151
8. Holub P, Swertz M, Reihs R, van Enckevort D, Müller H, Litton JE (2016) BBMRI-ERIC directory: 515 biobanks with over 60 million biological samples. Biopreserv Biobank 14:559–562. https://doi.org/10.1089/bio.2016.0088
9. Karen P, Stevanec M, Smerdu V, Cvetko E, Kubínová L, Eržen I (2009) Software for muscle fibre type classification and analysis. Eur J Histochem 53:87–95. https://doi.org/10.4081/ejh.2009.e11
10. Marco Salas S, Kuemmerle LB, Mattsson-Langseth C, Tismeyer S, Avenel C, Hu T, Rehman H, Grillo M, Czarnewski P, Helgadottir S, Tiklova K, Andersson A, Rafati N, Chatzinikolaou M, Theis FJ, Luecken MD, Wählby C, Ishaque N, Nilsson M (2025) Optimizing Xenium In Situ data utility by quality assessment and best-practice analysis workflows. Nat Methods 22:813–823. https://doi.org/10.1038/s41592-025-02617-2
11. Meznaric M, Cvetko E (2016) Size and proportions of slow-twitch and fast-twitch muscle fibers in human costal diaphragm. Biomed Res Int 2016:5946520. https://doi.org/10.1155/2016/5946520

12. Meznaric M, Eržen I, Karen P, Cvetko E (2018) Effect of ageing on the myosin heavy chain composition of the human sternocleidomastoid muscle. Ann Anat 216:95–99. https://doi.org/10.1016/j.aanat.2017.12.001
13. Mora M, Angelini C, Bignami F, Bodin AM, Crimi M, Di Donato JH, Felice A, Jaeger C, Karcagi V, LeCam Y, Lynn S, Meznaric M, Moggio M, Monaco L, Politano L, de la Paz MP, Saker S, Schneiderat P, Ensini M, Garavaglia B, Gurwitz D, Johnson D, Muntoni F, Puymirat J, Reza M, Voit T, Baldo C, Bricarelli FD, Goldwurm S, Merla G, Pegoraro E, Renieri A, Zatloukal K, Filocamo M, Lochmüller H (2015) The EuroBioBank network: 10 years of hands-on experience of collaborative, transnational biobanking for rare diseases. Eur J Hum Genet 23:1116–1123. https://doi.org/10.1038/ejhg.2014.272
14. Murgia M, Nogara L, Baraldo M, Reggiani C, Mann M, Schiaffino S (2021) Protein profile of fiber types in human skeletal muscle: a single-fiber proteomics study. Skelet Muscle 11:24. https://doi.org/10.1186/s13395-021-00279-0
15. Nolte KB (1991) Rhabdomyolysis associated with cocaine abuse. Hum Pathol 22:1141–1145. https://doi.org/10.1016/0046-8177(91)90267-S
16. Pasnoor M, Barohn RJ, Dimachkie MM (2014) Toxic myopathies. Neurol Clin 32:647–670. https://doi.org/10.1016/j.ncl.2014.04.009
17. Pette D, Staron RS (2000) Myosin isoforms, muscle fiber types, and transitions. Microsc Res Tech 50:500–509. https://doi.org/10.1002/1097-0029(20000915)50:6%3C500::AID-JEMT7%3E3.0.CO;2-7
18. Pinal-Fernandez I, Mammen AL (2016) Spectrum of immune-mediated necrotizing myopathies and their treatments. Curr Opin Rheumatol 28:619–624. https://doi.org/10.1097/BOR.0000000000000335
19. Schiaffino S, Reggiani C (2011) Fiber types in mammalian skeletal muscles. Physiol Rev 91:1447–1531. https://doi.org/10.1152/physrev.00031.2010
20. Schiaffino S, Rossi AC, Smerdu V, Leinwand LA, Reggiani C (2015) Developmental myosins: expression patterns and functional significance. Skelet Muscle 5:22. https://doi.org/10.1186/s13395-015-0046-6
21. Selvaraj V, Gollamudi LR, Sharma A, Madabushi J (2013) A case of cocaine-induced myopathy. Prim Care Companion CNS Disord 15. https://doi.org/10.4088/PCC.12l01451. PCC.12l01451
22. Ståhl PL, Salmén F, Vickovic S, Lundmark A, Navarro JF, Magnusson J, Giacomello S, Asp M, Westholm JO, Huss M, Mollbrink A, Linnarsson S, Codeluppi S, Borg Å, Pontén F, Costea PI, Sahlén P, Mulder J, Bergmann O, Lundeberg J, Frisén J (2016) Visualization and analysis of gene expression in tissue sections by spatial transcriptomics. Science 353:78–82. https://doi.org/10.1126/science.aaf2403
23. Tidball JG (2017) Regulation of muscle growth and regeneration by the immune system. Nat Rev Immunol 17:165–178. https://doi.org/10.1038/nri.2016.150
24. Umek N, Meznarič M, Šink Ž, Blagotinšek Cokan K, Prosenc Zmrzljak U, Horvat S (2025) In situ spatial transcriptomic analysis of human skeletal muscle using the Xenium platform. Cell Tissue

Res 399:291–302. https://doi.org/10.1007/s00441-024-03945-z

25. Williamson DL, Gallagher PM, Carroll CC, Raue U, Trappe SW (2001) Reduction in hybrid single muscle fiber proportions with resistance training in humans. J Appl Physiol 91:1955–1961. https://doi.org/10.1152/jappl.2001.91.5.1955
26. Wischnewski S, Thäwel T, Ikenaga C, Kocharyan A, Lerma-Martin C, Zulji A, Rausch HW, Brenner D, Thomas L, Kutza M, Wick B, Trobisch T, Preusse C, Haeussler M, Leipe J, Ludolph A, Rosenbohm A, Hoke A, Platten M, Weishaupt JH, Sommer CJ, Stenzel W, Lloyd TE, Schirmer L (2024) Cell type mapping of inflammatory muscle diseases highlights selective myofiber vulnerability in inclusion body myositis. Nat Aging 4:969–983. https://doi.org/10.1038/s43587-024-00645-9

Figures

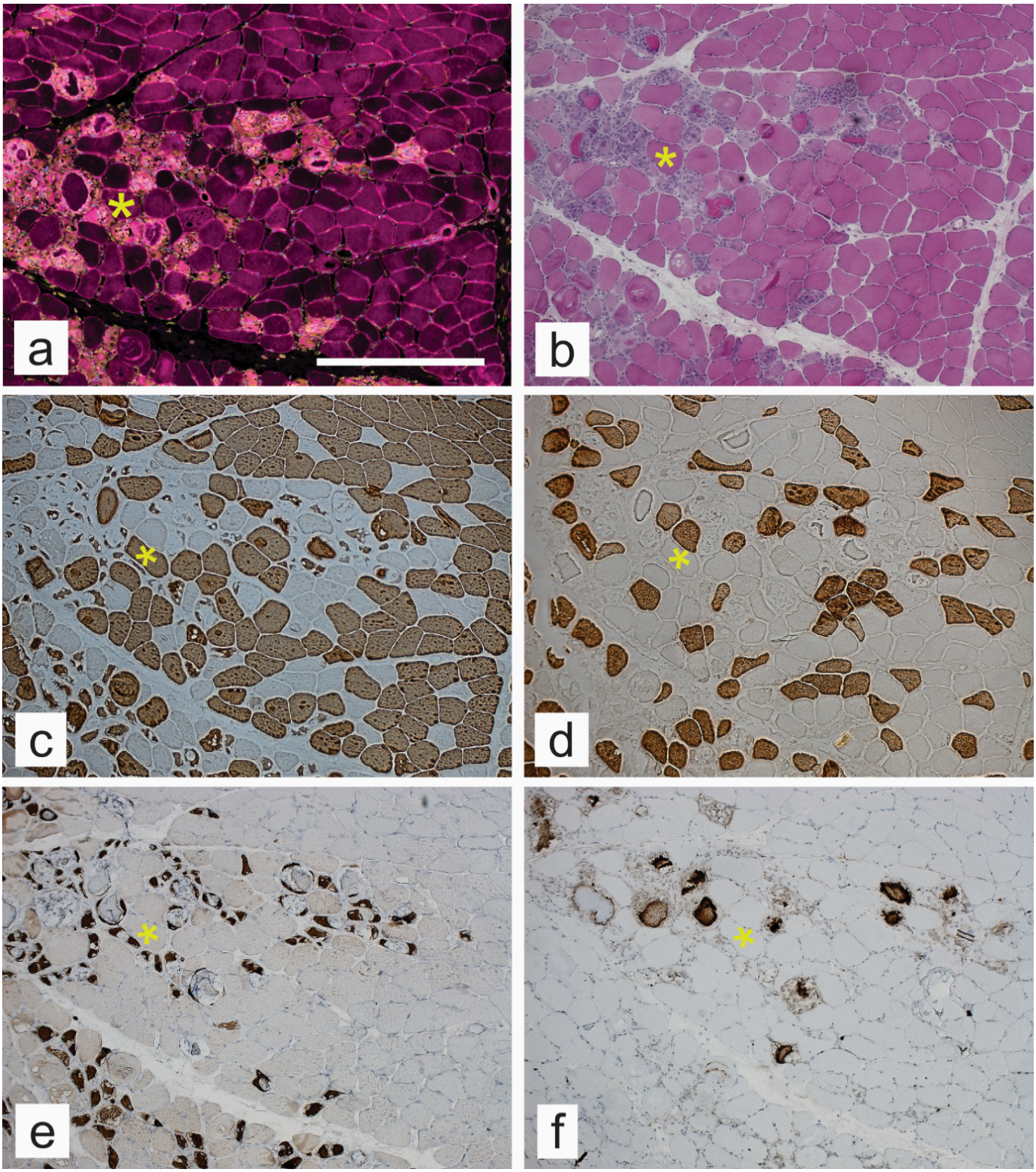


Figure 1

Representative lesion field analysed by Xenium and corresponding serial sections used for fibre annotation. (a) Xenium multimodal image. (b) Post-run hematoxylin and eosin (H&E) image of the same Xenium section. (c) BA-D5 immunostaining identifying type 1 fibres. (d) SC-71 immunostaining identifying type 2 (MyHC2a/2x-positive) fibres. (e) Neonatal MyHC immunostaining highlighting

regenerative fibres. (f) C5b9 immunostaining supporting identification of necrotic fibres. The yellow asterisk marks the same muscle fibre across all panels. The white scale bar corresponds to 500 µm

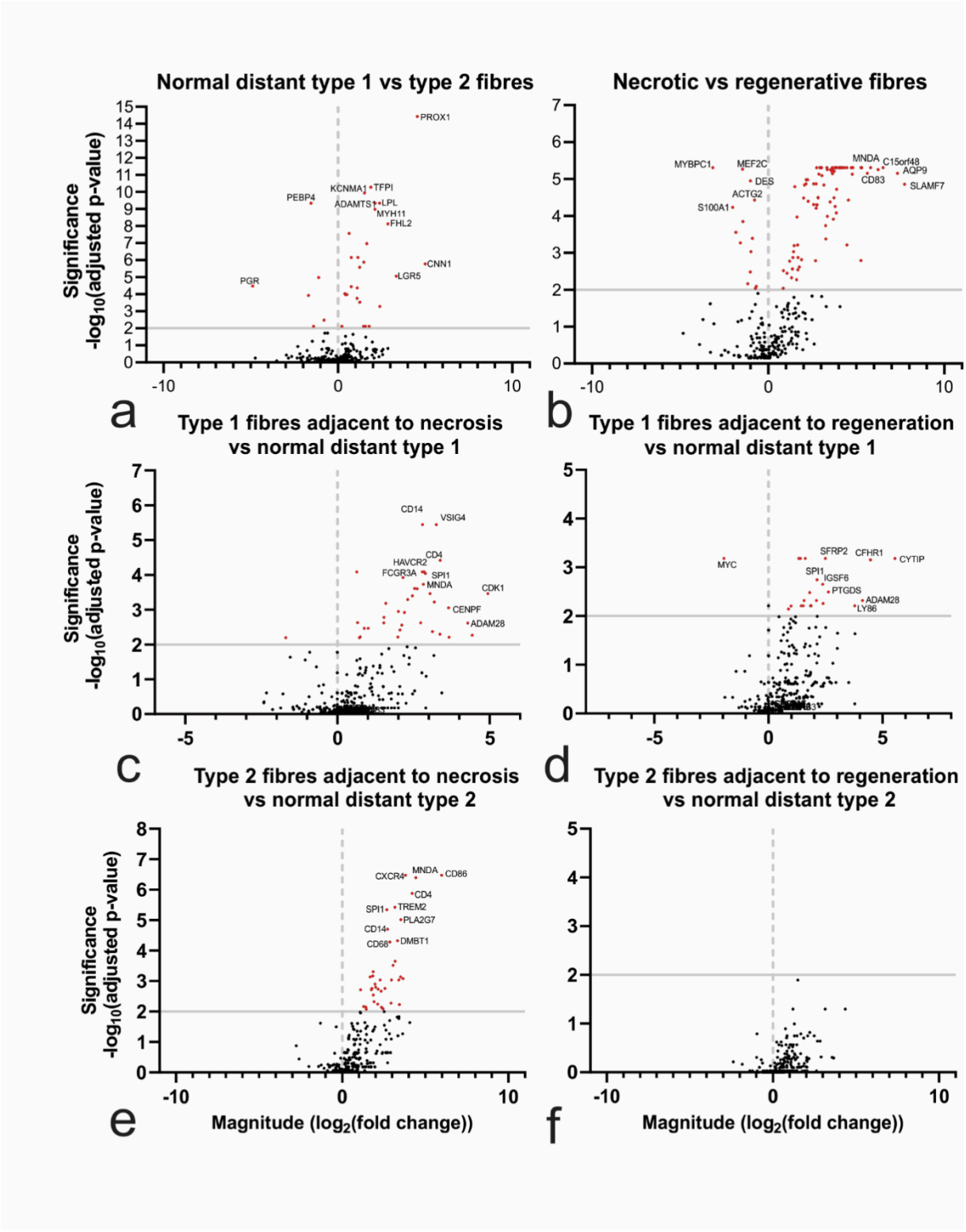


Figure 2

Volcano plots for pairwise differential-expression contrasts across fibre states. (a) Distant normal type 1 vs distant normal type 2 fibres. (b) Necrotic vs regenerative fibres. (c) Type 1 fibres adjacent to necrosis

vs distant normal type 1 fibres. (d) Type 1 fibres adjacent to regeneration vs distant normal type 1 fibres. (e) Type 2 fibres adjacent to necrosis vs distant normal type 2 fibres. (f) Type 2 fibres adjacent to regeneration vs distant normal type 2 fibres. The x-axis shows log2 fold change and the y-axis shows -log10 (adjusted p value). The dashed vertical line marks log2 fold change = 0, and the horizontal line marks the false discovery rate threshold q = 0.01. Red points denote transcripts significant at q < 0.01; panel (f) contains no significant transcripts at the predefined threshold

Supplementary Files

This is a list of supplementary files associated with this preprint. Click to download.

- SupplementaryTableS1.xlsx
- SupplementaryTableS2.xlsx
- SupplementaryTableS3.xlsx
- SupplementaryTableS4.xlsx
- SupplementaryTableS5.xlsx
- SupplementaryTableS6.xlsx
- SupplementaryTableS7.xlsx
- SupplementaryTableS8.xlsx
- SupplementaryTableS9.xlsx
- SupplementaryTableS11.xlsx
- SupplementaryTableS10.xlsx
- SupplementaryTableS15.xlsx
- SupplementaryTableS13.xlsx
- SupplementaryTableS12.xlsx
- SupplementaryTableS14.xlsx
- Supplementarytablecaptions.docx